# Tizian Bucher<sup>1</sup>

Advanced Manufacturing Laboratory, Department of Mechanical Engineering, Columbia University, New York, NY 10027 e-mail: tb2430@columbia.edu

# **Steven Cardenas**

Advanced Manufacturing Laboratory, Department of Mechanical Engineering, Columbia University, New York, NY 10027 e-mail: sac2241@columbia.edu

## Ravi Verma

Materials & Manufacturing Tech, Boeing Research & Technology, Berkeley, MO 63134 e-mail: ravi.verma2@boeing.com

# Wayne Li

Boeing Company, Ridley Park, PA 19078 e-mail: wayne.w.li@boeing.com

## Y. Lawrence Yao

Fellow ASME Advanced Manufacturing Laboratory, Department of Mechanical Engineering, Columbia University, New York, NY 10027 e-mail: yly1@columbia.edu

# Laser Forming of Sandwich Panels With Metal Foam Cores

Over the past decade, laser forming has been effectively used to bend various metal foams, opening the possibility of applying these unique materials in new engineering applications. The purpose of the study was to extend laser forming to bend sandwich panels consisting of metallic facesheets joined to a metal foam core. Metal foam sandwich panels combine the excellent shock-absorption properties and low weight of metal foam with the wear resistance and strength of metallic facesheets, making them desirable for many applications in fields such as aerospace, the automotive industry, and solar power plants. To better understand the bending behavior of metal foam sandwich panels, as well as the impact of laser forming on the material properties, the fundamental mechanisms that govern bending deformation during laser forming were analyzed. It was found that the well-established bending mechanisms that separately govern solid metal and metal foam laser forming still apply to sandwich panel laser forming. However, two mechanisms operate in tandem, and a separate mechanism is responsible for the deformation of the solid facesheet and the foam core. From the bending mechanism analysis, it was concluded on the maximum achievable bending angle and the overall efficiency of the laser forming process at different process conditions. Throughout the analysis, experimental results were complemented by numerical simulations that were obtained using two finite element models that followed different geometrical approaches. [DOI: 10.1115/1.4040959]

Keywords: laser forming, metal foam, sandwich panel, bending mechanism, numerical simulation

## 1 Introduction

Metal foam has long been acknowledged for its excellent shock and noise absorption properties, as well as its high strength to weight ratio [1,2]. Despite its desirable characteristics, metal foam alone is generally not suitable for structural applications because its thin cellular structure can easily be damaged and often makes the practical incorporation difficult. In many cases, it is, therefore, desirable to encapsulate metal foam within a shell of solid metal. Of particular interest are so-called "sandwich" panels, where plates of metal foam are "sandwiched" in between solid metal sheets. The metal sheets ("facesheets") not only protect the foam core from damage but also significantly improve the stiffness of the composite while maintaining a high strength to weight ratio.

Potential applications for sandwich panels with metal foam core range from various car components [3–5] to solar power plants [6] and train/ship structures [7,8]. Perhaps, the greatest potential for application exists in the aerospace industry. Specifically, sandwich panels could be used as turbine casings to arrest blades in case of a failure and reduce noise while maintaining low weight [9]. Metal foam sandwich panels could further be used in airplane "noses" to absorb impact energy from bird collisions [10]. In some applications, they could also replace honeycomb structures that are frequently used in modern airplanes. Unlike honeycomb structures, which are anisotropic and cannot be readily curved, metal foam is isotropic and can be bent to doubly curved shapes [2]. Moreover, the densities and geometries that can be used for honeycomb structures is limited, whereas

sandwich panels with metal foam core can be manufactured in a variety of different densities, cell shapes (using open/closed cell foams), and cell sizes [11].

The challenge associated with using candwich panels with

The challenge associated with using sandwich panels with metal foam core in industrial applications is that they must be manufactured to specific and, oftentimes, intricate shapes. It is possible to manufacture sandwich panels directly into the required shape using powder metallurgy processes [11]. This process involves creating a precursor material consisting of compressed metal and foaming agent powders, placing it between solid metal "facesheets," and bending the assembly to the desired shape. Afterward, the assembly is moved to a furnace, which causes the foaming agent to release a gas that turns the precursor into a foam. Elevated temperatures cause metallic bonds to form between the foam and adjacent facesheets. While feasible, the drawback of this process is that it requires molds both for the initial forming and subsequent heating. This limits the part size and makes the process very expensive for low production volumes. Furthermore, the structure and density of the resulting foam core is oftentimes irregular because it was produced in a nonuniform shape.

An alternative method to manufacture engineering parts is to start with generic shapes, such as flat panels, and subsequently bend them into the required shapes. This method is significantly cheaper and offers better control over the metal foam properties. At the same time, this method is challenging because sandwich panels with metal foam core are difficult to bend. Mechanical bending has been attempted, such as three-point bending [12,13] or die stamping [14] but caused many different types of defects and failures. Additionally, three-point bending has been attempted at elevated temperatures, yet no improvement was observed beyond slightly postponing the onset of failures in mechanical

Manuscript received March 30, 2018; final manuscript received July 18, 2018; published online August 31, 2018. Assoc. Editor: Hongqiang Chen.

<sup>&</sup>lt;sup>1</sup>Corresponding author.

bending at room temperature [15]. Although hydroforming allowed forming dome-shaped parts, it severely densified the metal foam core and thus diminished the favorable properties of the sandwich panel [16].

A viable alternative to the aforementioned processes is laser forming, since it is based on thermally induced mechanical deformation and requires no physical contact with the treated material. The process has successfully been used to bend a variety of different metal foams, such as closed-cell foams [17,18], open-cell foams [19], as well as foams with protective skins [20]. Yet, no attempt has been made to apply laser forming to sandwich panels with metal foam cores. Extending the laser forming study to sandwich panels is challenging because the interfaces and interactions between the facesheets and the foam core are critical to the overall material and must be taken into consideration. The existence of an interface significantly complicates the heat transfer and mechanics, and more involved numerical simulations are consequently required to understand these phenomena. These issues, along with a thorough discussion of the bending mechanisms and the applicable process window, are investigated in this study.

### 2 Background

2.1 Sandwich Panel Manufacture and Bending. Sandwich panels consist of three components: a foam core (metal foam in this study) and two solid metallic "facesheets" that are attached on either side of the foam core. In some studies, sandwich panels are referred to as materials in which the core and the facesheets are a single part. Examples are metal foams that develop protective skins during powder metallurgical processes [11,20]. More commonly, however, sandwich panels consist of facesheets and a foam core that are distinct entities and initially separated. These sandwich panels have stronger facesheets that better protect the foam core and increase the stiffness of the sandwich panel. Additionally, these sandwich panels offer a greater flexibility in material composition, since different material types and alloys can be used for the facesheets and the foam core combination.

To manufacture these sandwich panels, the facesheets need to be attached to the core, which can be achieved in different fashions. In this study, a typical method in which a precursor block consisting of compressed aluminum and foaming agent powders was used. The precursor is sandwiched between two facesheets and heated near the melting temperature of the metal powder. During heating, the foaming agent releases a gas that generates cavities inside the precursor and forms the foam. To ensure that the sandwich panel has a uniform thickness and that metallic bonds can establish between the foam and the facesheets, expansion in the direction of panel thickness is restricted during the foaming process [11].

While having an exceptional strength and stiffness, the resulting sandwich panels are extremely challenging to bend, due to several reasons. First, the major constituent of the sandwich panels is metal foam, which is unable to withstand the high tensile stresses that develop during mechanical deformation processes [18]. Hence, core shear failures are one of the most prevalent failure types seen in mechanical bending [2,12,13]. Second, sandwich panels are extremely stiff, and their moment of area *I* is substantially greater than the moment of area of a solid with the same cross-sectional area (Fig. 1), where *I* is calculated using

$$I = \int_{-s_0/2}^{s_0/2} z^2 y(z) dz \tag{1}$$

where  $s_0$  is the sheet thickness [2]. As a consequence, the sandwich panel has a much higher bending stiffness S than the corresponding solid as shown in

$$S = \frac{2EI}{l^3} = \frac{M}{l\delta} \tag{2}$$

where l is half the beam length, E is Young's Modulus, and  $\delta$  is the vertical deflection of the beam during bending [2]. Therefore, a greater bending moment M is required to achieve the same bending deflection  $\delta$ , which, in turn, increases the stresses in the foam core, making it even more prone to shear failures. High stresses also develop in the facesheets that can cause facesheet failures or wrinkling [2,13].

Third, deforming sandwich panels is exceedingly difficult due to the presence of the facesheet/foam interfaces. During mechanical bending processes, such as three-point bending, significant stress discontinuities develop at the interfaces due to the drastic difference in the material properties between the metal foam and the facesheets. Assuming bending occurs about the *x*-axis (see Fig. 2) and is achieved by a bending moment *M*, the normal strain at a distance *z* from the neutral axis can be written as  $\varepsilon_{22} = -z/R$  [21], where *R* is the radius of curvature. The normal stress (in *y*-direction) then becomes

$$\sigma_{22} = E\varepsilon_{22} = -\frac{Ez}{R} \tag{3}$$

where E is Young's modulus. The sign indicates that the deformation is compressive and tensile above and below the neutral axis, respectively. Since the radius of curvature is constant, the magnitude of the stress discontinuity depends on the difference in Young's modulus between the facesheet and the foam, which can readily reach a factor of 100. At the interface, this stress discontinuity is experienced as a shear traction and can cause delamination [12,13].

Finally, the interaction between the facesheet and the foam can cause additional undesirable effects. Due to the high compressive stresses that develop during mechanical bending, the facesheet can buckle into the foam core, compressing the foam to a fraction of its original thickness [2,13]. As a consequence, the foam loses a majority of its local compressibility and renders the sandwich useless for shock-absorption applications.

**2.2 Laser Forming.** Laser forming of solid sheet metal is well understood; several mechanisms explain the bending behavior at different process conditions [22]. The first bending mechanism, temperature-gradient mechanism (TGM), governs the scenario where the sample sheet thickness is relatively large compared to the laser spot size. Steep temperature gradients develop across the sheet thickness, and heating is highly localized underneath the laser source. As a consequence, the thermal expansion of the heated material is restricted by the cold surrounding material, and plastic compression occurs. Plastic compression is propagated along the entire laser scan, shortens the top of the sheet relative to the bottom, and ultimately bends the material toward the laser. The second mechanism, buckling mechanism (BM), governs the scenario where the laser spot is much larger than the sheet thickness, causing uniform heating across the thickness. The sheet again tries to expand but is hindered by the surrounding material, ultimately buckling away or toward the laser source. The buckled region is propagated along the laser scan, and the sheet eventually bends in the direction opposite to the buckling direction. The third mechanism, upsetting mechanism (UM), governs the same scenario as the BM, except the section is geometrically prevented from buckling and instead undergoes thickening.

For metal foams, it was shown that none of the aforementioned mechanisms exactly apply, and a modified temperature-gradient mechanism (MTGM) was proposed [18]. In the MTGM, a steep temperature gradient develops across the thickness just like in the TGM, but the compressive shortening near the top surface occurs via cell crushing as opposed to plastic compressive strains.

For sandwich panels with metal foam cores, the bending mechanism analysis becomes more involved. For one, the interaction between the facesheets and the metal foam must be taken into consideration. The facesheets tend to bend at a higher rate than

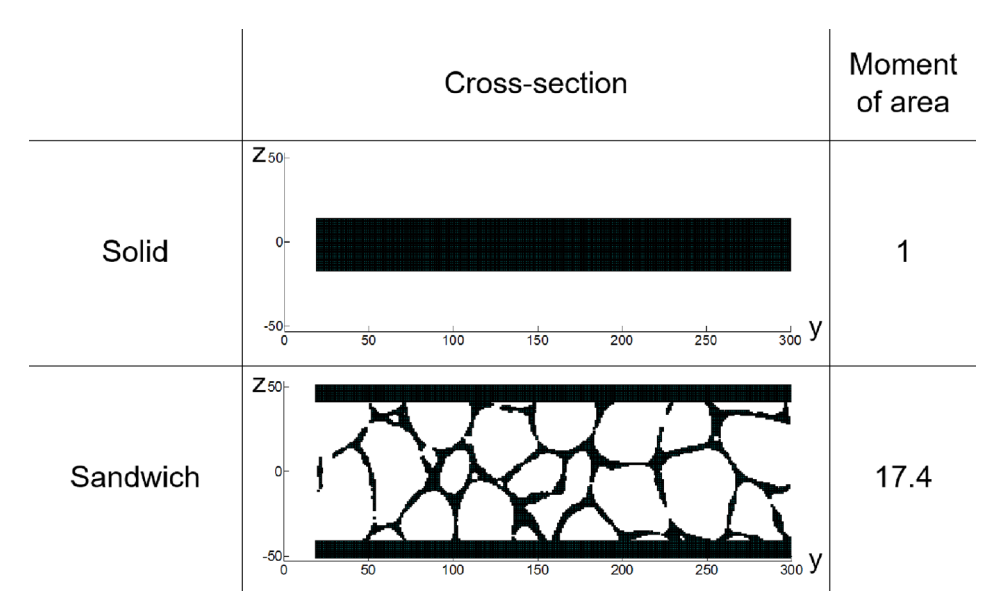


Fig. 1 An example showing a metal foam sandwich (89% porosity, total thickness 10 mm, facesheets thickness 1 mm), which has a 17.4 times higher moment of area about the *y*-axis than a solid with the same cross-sectional area (thickness 3.2 mm). Hence, metal foam sandwiches have a higher stiffness to bending deformation. The cross sections were divided into squares of 0.1 mm length, whose moment of area were calculated individually and added using the parallel axis theorem. The *y*- and *z*-axes refer to the number of squares per coordinate direction. The total number of squares was the same for the solid and sandwich.

the metal foam core and are thus "held back," which can give rise to stresses at the interface. Moreover, there is no bending mechanism that is valid both for solid sheet metal and metal foam, and hence, there is no mechanism that can explain the bending behavior of the entire sandwich panel. The TGM and the MTGM, for instance, cannot govern bending of the entire sandwich panel, since the foam deformation is not mainly based on plastic compression, and the facesheet cannot undergo crushing, respectively. The BM cannot be valid either, since the thickness of the composite is too large to undergo buckling. The UM can only partially explain the sandwich deformation for a set of process conditions, as will be shown, but does not explain how the foam core can bend without undergoing fracture. It turns out that the sandwich panel deformation can be explained by a combination of two mechanisms, which interact and give rise to a new phenomenon at the interface between the top facesheet and the foam core.

## 3 Numerical Simulation

Several methods can be used to model sandwich panels. The simplest method is to model the sandwich as a block, divide it into three regions, and assign facesheet and foam properties to the corresponding regions [23]. Though extremely simple, the disadvantage of this method is that the facesheet and core are always rigidly connected, and the heat transfer between them is assumed to be perfect (infinite conductance). Since the facesheet and foam core are not fully melted during manufacturing, however, the interface contains microvoids, and the adhesion is imperfect. Hence, a finite thermal conductance is to be expected, which can only be taken into account by models where the facesheets and the foam core are initially detached.

Initially detached models require a joining method, of which there are again several alternatives. A simplistic method involves joining the facesheet and foam core using tie constraints or contact interactions [13,16]. Both methods can model contact resistances, yet do not allow for any delamination to occur. Cohesive surfaces have the same thermal capabilities but also allow for delamination to occur when specified damage parameters are exceeded [24]. The same result can be achieved by inserting a thin layer (e.g.,  $10 \, \mu m$ ) at the interface consisting of cohesive

elements, with the additional benefit that delamination can be monitored and visualized [25]. Even though delamination did not occur in the current study, this approach was used for both interfaces, in anticipation of future studies where delamination effects become important.

The cohesive element approach assumes the interface layer to be infinitesimally thin, and the deformation is described in terms of the tractions t and the displacement discontinuity u across the interface. The tractions and displacements are linearly related through the stiffness matrix K

$$\begin{bmatrix} t_n \\ t_s \\ t_t \end{bmatrix} = \begin{bmatrix} K_{nn} & 0 & 0 \\ 0 & K_{ss} & 0 \\ 0 & 0 & K_{tt} \end{bmatrix} \begin{bmatrix} u_n \\ u_s \\ u_t \end{bmatrix}$$
(4)

where the subscripts n, s, t refer to the normal, first and second shear directions, respectively. The stiffness of the cohesive layer is set very high to avoid affecting the response of the sandwich [26].

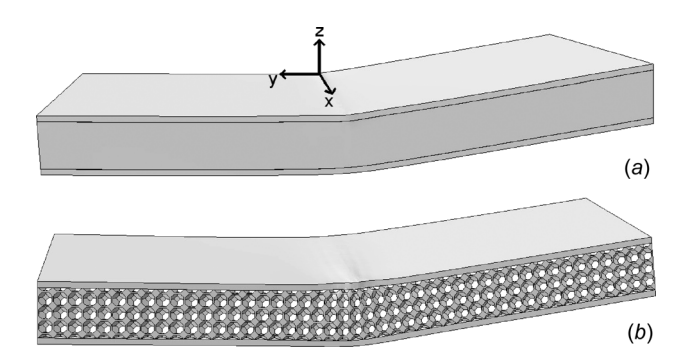


Fig. 2 Two different geometries were used to model the foam core: (a) solid geometry ("equivalent model"), whereby foam properties were assigned, and (b) Kelvin cell geometry ("Kelvin model"), where each cavity was approximated by a Kelvin-cell. Not visible are the cohesive layers that were inserted between the facesheets and the foam core.

To simulate the imperfect heat transfer at the interfaces, temperature-dependent conductance values G(T) were assigned. G(T) data are currently only available for metals in direct contact that are subjected to a pressure. Several references suggest an exponential increase of G with temperature T [27–29]. For sandwich panels, the conductance should be greater than in direct contact because of the presence of metallic bonds; however, due to the lack of available reference data, the G(T) relationship from Ref. [27] was used.

The laser-forming simulation was performed in an uncoupled manner, using the thermal results as input to the mechanical analysis. The facesheets were modeled using Von Mises' yield criterion, and temperature-dependent material properties were extracted from Ref. [30]. Simulations were implemented in the finite element software ABAQUS using DC3D20 and C3D20R elements for the thermal and mechanical analysis, respectively. The top and bottom facesheets were modeled with three and two elements through the thickness, respectively.

The metal foam was modeled in two different ways. In the first method ("equivalent model"), shown in Fig. 2(a), the foam was modeled as a solid, and metal foam properties were assigned. Yielding was assumed to occur due to deviatoric and hydrostatic stresses, pursuant the criterion

$$F = \left[ \frac{1}{1 + (\alpha/3)^2} \left( \sigma_e^2 + \alpha^2 \sigma_m^2 \right) \right]^{1/2} - Y \le 0$$
 (5)

where  $\sigma_e$  is the Von Mises' equivalent stress,  $\sigma_m$  the mean stress, Y the yield strength, and  $\alpha$  the aspect ratio of the yield surface [31]. When F < 0, the material behavior is elastic, and when F = 0, plastic deformation occurs pursuant to the following flow rule:

$$\dot{\varepsilon}_{ij}^{p} = \frac{\dot{Y}}{H} \frac{\partial F}{\partial \sigma_{ii}} \tag{6}$$

where  $\dot{e}_{ij}^P$  is the plastic strain rate, and H is the hardening modulus defined as

$$H = \frac{\sigma_e}{\hat{\sigma}} h_\sigma + \left(1 - \frac{\sigma_e}{\hat{\sigma}}\right) h_p \tag{7}$$

where  $h_{\sigma}$  and  $h_p$  are the tangent moduli in uniaxial and hydrostatic compression, respectively, and  $\hat{\sigma}$  is the equivalent stress equal to the first term in Eq. (5). The assumptions of this model and the sources for the material data are discussed in detail in Refs. [17] and [18]. The x and y mesh refinement was the same as in Ref. [18], in z-direction the mesh was more refined toward the interfaces and coarser toward the center of the foam. In the second method ("Kelvin model"), the foam cavity was approximated by a Kelvin cell, shown in Fig. 2(b), and solid AlSi10 properties were assigned. The element types and meshing technique were the same as in Ref. [18], with the exception that a cavity size of 2 mm was used, yielding a density of  $700 \, \text{kg/m}^3$ .

In the equivalent model, the cohesive layer was meshed with COH3D8 elements that were half the size of the adjacent metal foam elements. In the Kelvin model, the same element size was used for the cohesive layer as in the adjacent metal foam elements. The thermal and mechanical boundary conditions were the same as in prior analyses [17,18], and an absorption coefficient of A = 0.6 was used [32].

## 4 Experimental Methods

Sandwich panels manufactured by Havel Metal Foam Gmbh were used in this study, consisting of AW 5005 facesheets and AlSi10 metal foam core. The thickness of the sandwiches was 10 mm, and the average density of the metal foam was measured

to be  $700 \,\mathrm{kg/m^3}$ . The manufacturing method was discussed in Sec. 2.1. Sandwich specimens were cut to a length of  $100 \,\mathrm{mm}$  and a width of  $35 \,\mathrm{mm}$  and mounted onto a thermally insulated stage as shown in Fig. 3. A CO<sub>2</sub> laser with a wavelength of  $10.6 \,\mu\mathrm{m}$  was used to scan the specimens in x-direction. To improve the naturally poor absorption of  $10.6 \,\mu\mathrm{m}$  radiation in aluminum [33], the specimens were coated in black graphite paint. The specimens were cooled to room temperature after each laser scan, at which point the deflection was measured with a dial indicator.

Two different approaches were taken during the determination of the process conditions. In the first approach, inspiration was drawn from multilayer composite laser forming studies [34], in which the TGM was induced in the top layer, and the remaining sections of the composite were bent by the resulting bending moment. In the second approach, it was attempted to bend the entire sandwich panel through a laser forming mechanism by subjecting the entire section to a steep temperature gradient. For both approaches, bending was successful, but the bending mechanisms turned out to be different than anticipated, which will be discussed later. The first approach yielded a small spot size of D=4 mm with a high scan speed of v=30 mm/s, whereas the second approach yielded a large spot size of D=12 mm and a lower scan speed of v=10 mm/s. The power was kept at P=800 W to maintain a constant area energy AE=P/Dv.

Since both process conditions give rise to fundamentally different bending mechanisms, most of this study was dedicated to the comparison of the two conditions. However, the process window is not limited to these two conditions, and laser forming can also be achieved with intermediate laser spot sizes between D = 4–12 mm and scan speeds between v = 10–30 mm/s, as will be demonstrated in Sec. 5.3.

The temperatures on the bottom surface of the sandwich were measured using an IR camera. The IR camera was mounted underneath the specimen, and an aluminum shield was added to the stage to avoid damaging the IR camera. The maximum frame rate of 120 Hz was used, which provided sufficient detail to capture

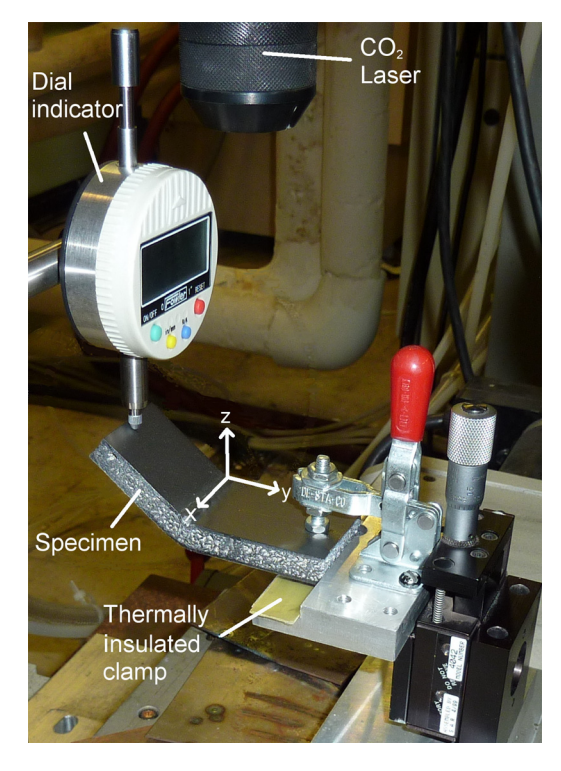


Fig. 3 Experimental setup. The specimens were scanned in x-direction, and a thermally insulating material was inserted between the specimen and the holder. The dial indiactor was removed during laser scans.

the temperature–time history. The spatial resolution of the IR camera is roughly  $0.1\,\mathrm{mm}$  at the distance operated, and the temperature resolution is  $0.1\,\mathrm{K}$ .

### 5 Results and Discussion

**5.1 Bending Mechanism.** To study the bending mechanism, sandwich specimens and "isolated" facesheets that were removed from the sandwich were both laser formed to about 15 deg. Then, the typical cross section of the sandwich specimens (Figs. 4(a) and 4(b)) were compared with cross section of isolated facesheets (Figs. 4(c) and 4(d)). The process conditions used for (a) and (c) were a small spot size of  $D=4\,\mathrm{mm}$  with a scan speed  $v=30\,\mathrm{mm/s}$ , and for (b) and (d) a large spot size of  $D=12\,\mathrm{mm}$  with a scan speed  $v=10\,\mathrm{mm/s}$ . The power and area energy were constant at  $P=800\,\mathrm{W}$  and  $AE=6.67\,\mathrm{J/mm^2}$ , respectively.

The bending of the isolated facesheets is governed by well-known bending mechanisms. At  $D=4\,\mathrm{mm}$ , some thickening occurred on the top surface (Fig. 4(c)), which is an established consequence of TGM-dominated bending [35]. At  $D=12\,\mathrm{mm}$  (Fig. 4(d)), there was insignificant change in the facesheet thickness, and the spot size was substantially greater than the facesheet thickness, indicating that the BM is the governing mechanism [22].

In comparison, it is evident that the bending of sandwich panels is governed by different mechanisms, since the cross section look quite different under both process conditions. At  $D=12\,\mathrm{mm}$  (Fig. 4(b)), the top facesheet no longer bent via the BM because it was prevented from buckling by the attached metal foam. Instead, the facesheet was thickened, a response that is indicative of the well-established UM. The temperature distributions across the thickness, shown in Fig. 5 as the laser passes, confirm this finding. Both in the isolated and sandwich configuration, there was hardly any temperature gradient across the top facesheet, speaking in favor of the BM and the UM, for each configuration respectively.

At D = 4 mm (Fig. 4(a)), the top facesheet in the sandwich configuration thickened not just upward but also downward, which is uncharacteristic for the TGM and suggests that a different bending

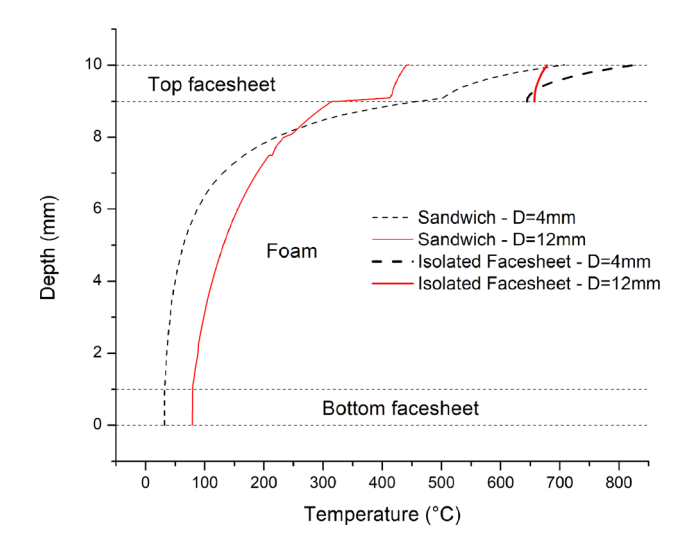


Fig. 5 Simulated temperature distributions at a cross section (yz-plane) as the laser passes, both in the entire sandwich (equivalent sandwich model) and in an isolated facesheet. At  $D=4\,\mathrm{mm}$  and  $v=30\,\mathrm{mm/s}$ , a steep temperature gradient exists in the top facesheet, regardless of whether the facesheet is isolated or in sandwich configuration, indicating that the TGM is always the governing mechanism. At  $D=12\,\mathrm{mm}$  and  $v=10\,\mathrm{mm/s}$ , there is hardly any gradient over the top facesheet in both scenarios, indicating that the BM and the UM govern in the isolated and sandwich configurations, respectively.

mechanism governs deformation. The thermal results from Fig. 5 suggest the contrary, however, since a steep temperature gradient developed across the top facesheet regardless of whether it was isolated or attached to the foam core.

Further evidence can be drawn from the experimental and numerical results in Fig. 6, showing the temperature history at the bottom sandwich panel surface at the scan line. At D=12 mm, a substantial amount of heat was transferred across the sandwich.

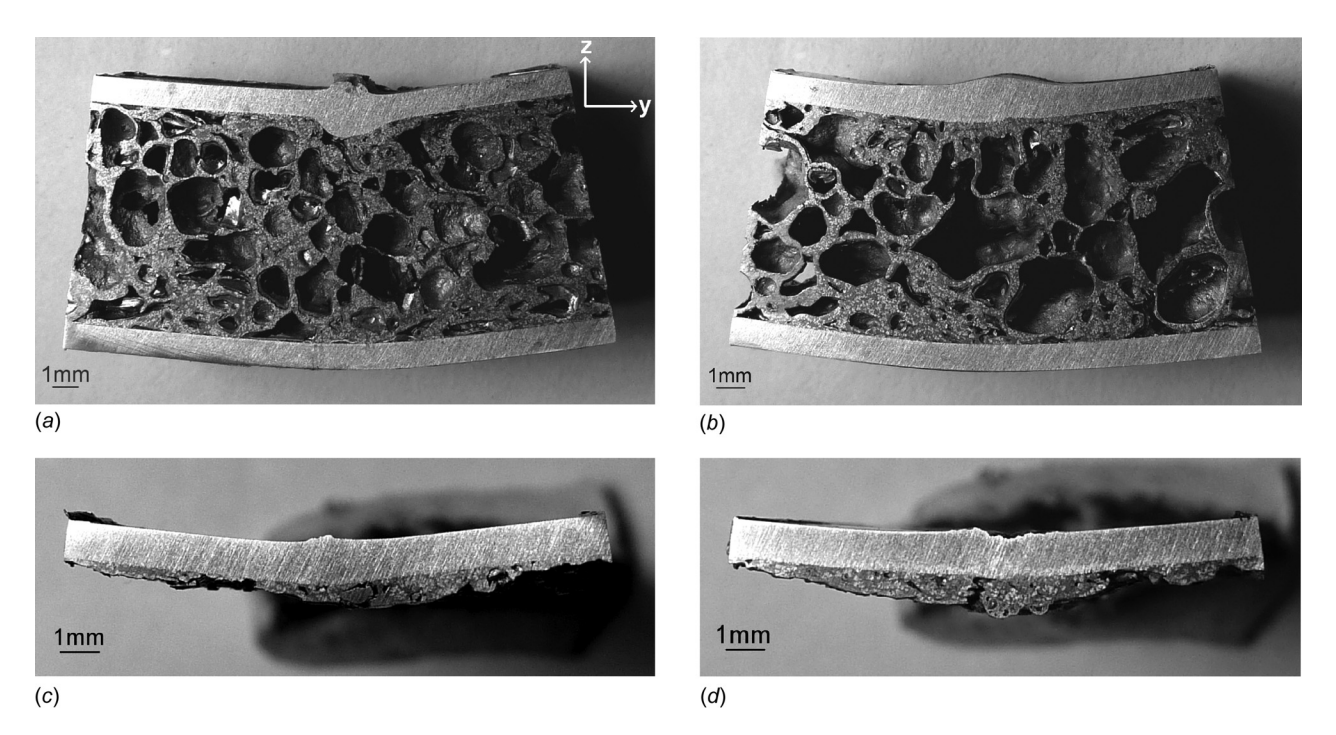


Fig. 4 Cross sections of sandwich panels scanned at (a)  $D=4 \,\mathrm{mm}$  and  $v=30 \,\mathrm{mm/s}$  (100 scans) and (b)  $D=12 \,\mathrm{mm}$  and  $v=10 \,\mathrm{mm/s}$  (24 scans), and cross section of isolated facesheets scanned at (c)  $D=4 \,\mathrm{mm}$  and  $v=30 \,\mathrm{mm/s}$  (7 scans), and (d)  $D=12 \,\mathrm{mm}$  and  $v=10 \,\mathrm{mm/s}$  (6 scans). The power and area energies were  $P=800 \,\mathrm{W}$  and 6.67 J/mm² in all cases, respectively, and the final bending angle was 15 deg. The top facesheet bent via the TGM in (a) and (c), the BM in (d), and the UM in (b).

This indirectly implies that the top facesheet heated up uniformly, again suggesting that the UM governed bending of the top facesheet. At  $D=4\,\mathrm{mm}$ , on the other hand, little heat reached the bottom sandwich surface, suggesting the presence of a temperature drop in the top facesheet, which gives rise to the TGM. It must be noted that in the experiment, a laser shield was placed very close to the bottom sandwich surface to protect the IR camera. This shield absorbed some heat and is responsible for the discrepancy between the experimental and numerical peak temperatures. Also, there is a significant temperature drop across the top interface, which can be attributed to the finite interface conductance. The temperature drop was more significant at  $D=12\,\mathrm{mm}$  than at  $D=4\,\mathrm{mm}$  due to the exponential temperature-dependence of the interface conductance G(T).

Thus far, the bending mechanism analysis was solely focused on the top facesheet, and evidence was found that the TGM and UM govern facesheet bending at  $D=4\,\mathrm{mm}$  and  $D=12\,\mathrm{mm}$ , respectively. The question now becomes how the rest of the sandwich panel bends. Two pieces of evidence show that the foam core actively bends through a laser forming mechanism as well, rather than bending solely because of the bending moment exerted by the top facesheet. First, steep temperature gradients develop across the foam during the laser scan as shown in Fig. 5, both at  $D=4\,\mathrm{mm}$  and  $D=12\,\mathrm{mm}$ . Second, the metal foam undergoes some densification during the laser scan as shown in Figs. 7(a) and 7(b), which is identical to the densification occurring during laser forming of free-standing metal foam [18]. The density changes were calculated using

$$\frac{\rho}{\rho_0} = e^{-(\epsilon_{11} + \epsilon_{22} + \epsilon_{33})} = e^{-(\epsilon_{ii})} \tag{8}$$

where  $\rho_0$  is the initial density and  $\varepsilon_{ii}$  are the normal strain components [14]. The initial density  $(\rho=\rho_0)$  is represented by 100%. Both results imply that the metal foam bent via the MTGM [18]. Experimental results confirm this finding, since some cell-crushing can be seen at small bending angles (Figs. 4(a) and 4(b)), and especially at large bending angles (see Sec. 5.2).

Therefore, both the top facesheet and foam core actively contribute to the bending deformation through different bending mechanisms. The last sandwich component requiring an analysis is the bottom facesheet. According to Fig. 5, there is no

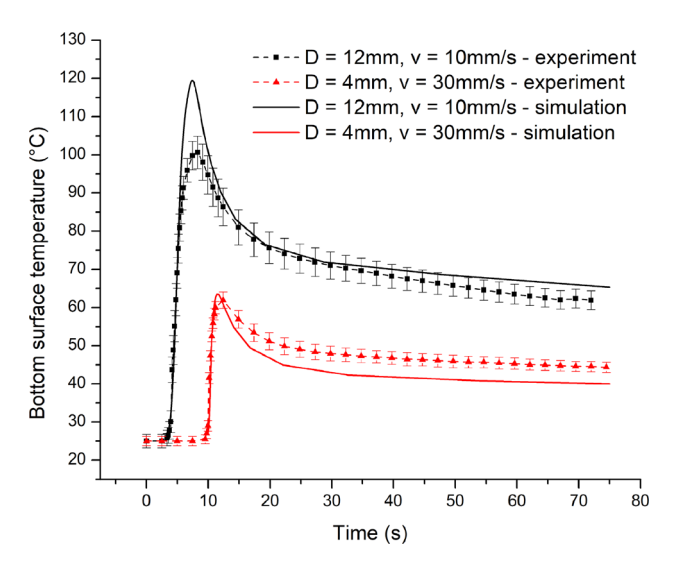


Fig. 6 Experimental and numerical temperature histories on the bottom sandwich panel surface at  $D=4\,\mathrm{mm}$  and  $D=12\,\mathrm{mm}$ . At  $D=12\,\mathrm{mm}$  there is a more significant temperature rise, indicating that more heat is transferred across the top facesheet. At  $D=4\,\mathrm{mm}$ , little heat reaches the bottom surface, implying the presence of a temperature gradient in the top facesheet.

temperature gradient across the bottom facesheet, and the amount of heating is low as well. Hence, the bottom facesheet is the only component of the sandwich panel that does not actively contribute to bending. Instead, it is bent mechanically by the bending moment exerted by the foam core and the top facesheet.

Having discussed the bending mechanisms, it becomes clear why laser-formed sandwich panels do not undergo any failures mentioned in Sec. 2.1. Core shear failures do not occur because the foam deformation through the MTGM is mostly compressive [18]. Similarly, buckling of the top facesheet does not occur, since the top facesheet undergoes compressive shortening via the TGM. Facesheet wrinkling does not occur either because the facesheets are too thick or bottom facesheet failures are prevented by heat-induced softening. Facesheet delamination can occur, depending on the joining method. In this study, a very strong joining method was used, which did not give rise to any delamination.

A further topic requiring discussion is the thickening on the bottom surface of the top facesheet (Fig. 4(a)). Two mechanisms can be held responsible for this behavior. First, the metal foam densifies, as shown in Figs. 7(a) and 7(b), and the associated volume reduction leaves a void in the foam to be filled. Since the adhesion between the top facesheet and the metal foam remains intact, the facesheet must fill this void, which it can readily accomplish because it is subject to high compressive stresses and also softened due to the laser-induced heating. Second, the top facesheet expands downward right as the laser passes. Figure 8 shows the strain distribution  $\varepsilon_{33}$  in z-direction (a) right before the laser passes, (b) while the laser passes and (c) at the end of the laser scan. Immediately before the laser passes, the top facesheet starts expanding uniformly. As the laser passes, the facesheet rapidly expands both upward and downward, inducing a compressive strain in the metal foam underneath. Meanwhile, the foam undergoes some compressive deformation of its own through the MTGM, thereby "pulling" the facesheet down and inducing a

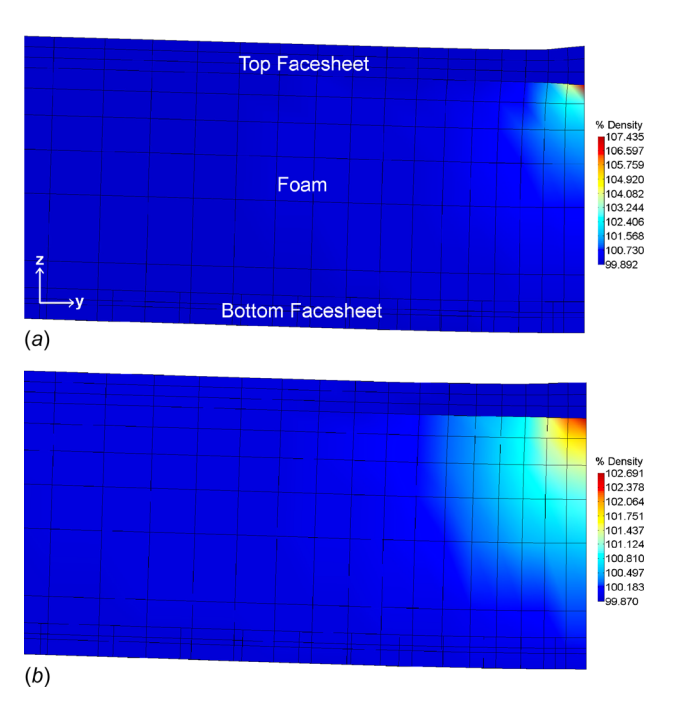


Fig. 7 Density distribution after a laser scan at (a)  $D=4\,\mathrm{mm}$  and  $v=30\,\mathrm{mm/s}$ , and (b)  $D=12\,\mathrm{mm}$  and  $v=10\,\mathrm{mm/s}$ . The initial density is 100%. At both conditions, the foam core densified as postulated by the MTGM. At  $D=4\,\mathrm{mm}$ , the densification has a higher magnitude but occurs more locally. At  $D=12\,\mathrm{mm}$ , densification occurs over a much greater area, allowing for a more efficient deformation at large bending angles. A deformation scaling factor of 5 was used. Half of the specimen is shown due to symmetry.

tensile strain in the facesheet. This condition is maintained until the end of the laser scan, as shown in Fig. 8(c).

**5.2 Bending Efficiency and Limit.** In Sec. 5.1, it was shown that small (D=4 mm) and large (D=12 mm) laser spot sizes induce different bending mechanisms in the top facesheet. The

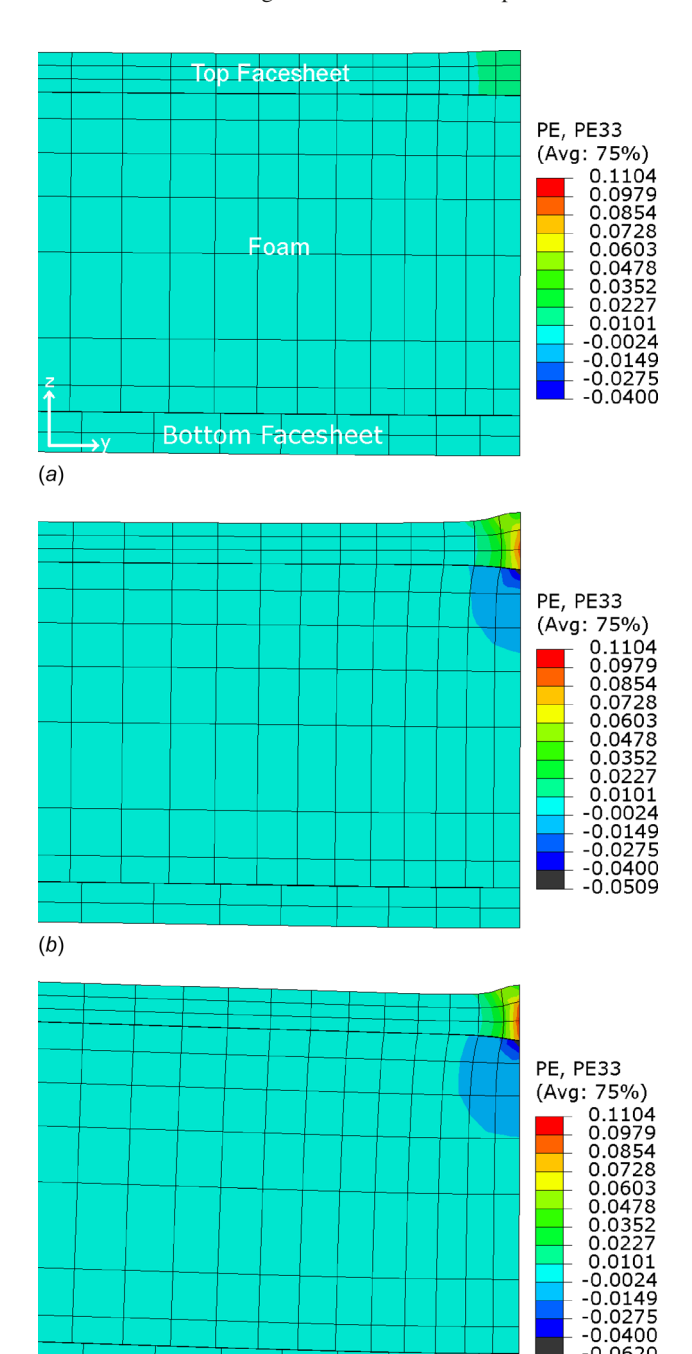


Fig. 8 Vertical plastic strain distribution in z-direction ( $\epsilon_{33}$ ) at the scan line at D=4 mm and v=30 mm/s (a) right before the laser passes, (b) as the laser passes, and (c) after the laser scan. Right as the laser passes, the top facesheet (top three element layers) expands upward and downwards near the scan line, compressing the foam underneath. The foam, in turn, densifies due to the MTGM and "pulls" the facesheet down, causing tensile strains in the top facesheet. A deformation scaling factor of 5 was used. Half of the specimen is shown due to symmetry.

(c)

bending mechanisms, in turn, significantly impact both the bending efficiency and the bending limit.

Figure 9 shows that the bending angles achieved at  $D=12 \,\mathrm{mm}$  were more than twice the bending angles achieved at  $D=4 \,\mathrm{mm}$  over 8 laser scans, even though the area energy was constant in both cases (AE = 6.67 J/mm<sup>2</sup>). These results clearly suggest that bending is significantly more efficient at larger laser spot sizes.

To explain the trends observed in Fig. 9, the plastic compressive strain distributions in y-direction ( $\varepsilon_{22}^p$ ) were analyzed over a cross section of the sandwich panel. At  $D=4\,\mathrm{mm}$  (Fig. 10(a)), large compressive strains developed at the center of the top facesheet due to intense heating and the large thermal expansion forces characteristic of the TGM. The remaining facesheet segments contributed much less to compressive deformation, and the plastically deformed area was generally localized near the laser scan line. At  $D=12\,\mathrm{mm}$  (Fig. 10(b)), the plastically deformed region extended further from the laser scan line, and the compressive strains were more uniformly distributed throughout the top facesheet. Hence, bending was more efficient at  $D=12\,\mathrm{mm}$  because a larger segment of the top facesheet contributed to compressive shortening.

Furthermore, bending was more efficient at D=12 mm because the foam core bent more efficiently via the MTGM. Unlike at D=4 mm (Fig. 10(a)), where the foam only underwent plastic compression adjacent to the scan line, the plastically compressed region was much larger at D=12 mm (Fig. 10(b)). The same conclusion can be drawn from the densification plots in Figs. 7(a) and 7(b), as well as experimental results at large bending angles (Fig. 11).

Finally, bending was more efficient at  $D=12\,\mathrm{mm}$  because the bottom facesheet reached higher temperatures during the laser scan, as shown in Fig. 6, and consequentially underwent a higher amount of heat-induced softening than at  $D=4\,\mathrm{mm}$ .

Similar to the bending efficiency, the maximum achievable bending angle is very sensitive to the laser spot size. At D=4 mm, the maximum bending angle is merely  $\sim 15$  deg, as shown in Fig. 4(a). Large bending angles can exclusively be achieved by performing multiple parallel laser scans. In Fig. 12(a), for instance, two scans were performed per scan line, and each scan line was offset by 1 mm. At D=12 mm, on the other hand, bending angles up to 65 deg and beyond can be achieved over a single scan line as shown in Fig. 12(b).

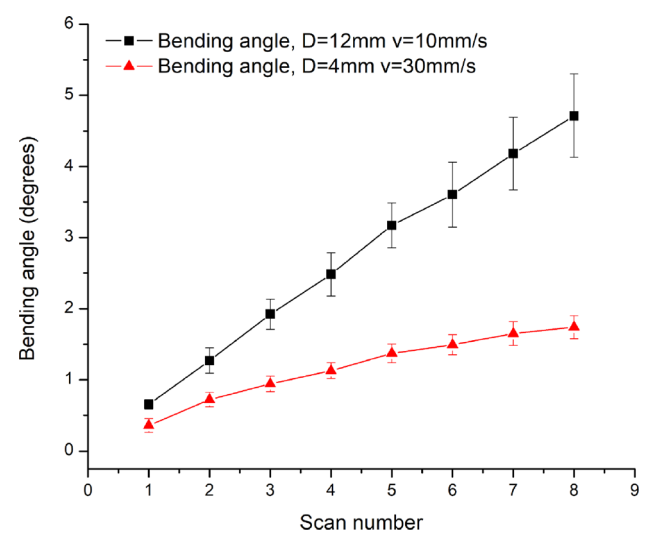
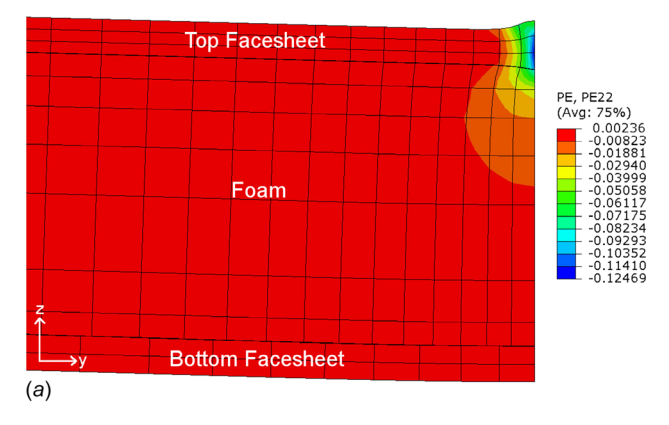


Fig. 9 Experimental bending angles over eight scans at  $D=4\,\mathrm{mm}$  with  $v=30\,\mathrm{mm/s}$ , and  $D=12\,\mathrm{mm}$  with  $v=10\,\mathrm{mm/s}$ . The power and area energy are constant at  $P=800\,\mathrm{W}$  and AE = 6.67 J/mm², respectively. The bending angles are averaged over five specimens, standard errors are shown. At  $D=12\,\mathrm{mm}$ , bending is more efficient than at  $D=4\,\mathrm{mm}$ .



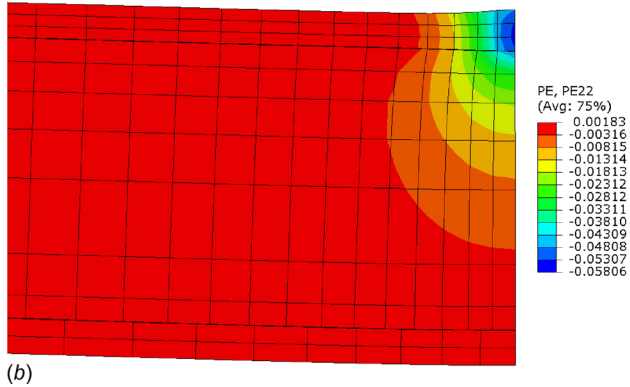


Fig. 10 Plastic strain distribution after a laser scan at (a)  $D=4\,\mathrm{mm}$  with  $v=30\,\mathrm{mm/s}$  and (b)  $D=12\,\mathrm{mm}$  with  $v=10\,\mathrm{mm/s}$ . At  $D=4\,\mathrm{mm}$ , significant compressive shortening only occurred over a small segment of the top facesheet (top three element layers), unlike at  $D=12\,\mathrm{mm}$ , where the entire top facesheet contributed to compressive shortening, and compressive strains extended further from the laser scan line. A deformation scaling factor of 5 was used. Half of the specimen is shown due to symmetry.

One cause for the different limiting behaviors is the bending mechanism that governs the deformation of the top facesheet. At D=4 mm, the top facesheet bends via the TGM, and considerable thickening occurs over the small area around the laser scan line (Fig. 4(a)). This thickening causes a significant drop in the bending angle increment  $\Delta\alpha$ , since  $\Delta\alpha$  is proportional to the inverse of

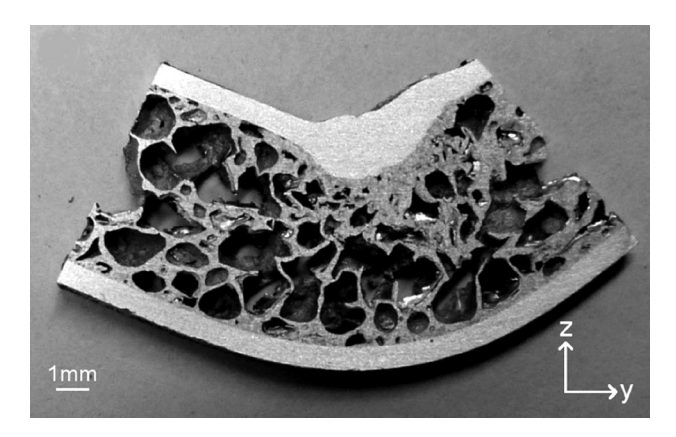


Fig. 11 Cross section of a sandwich specimen bent to 65 deg at  $D=12\,\mathrm{mm}$  and  $v=10\,\mathrm{mm/s}$ . The top facesheet thickened significantly, and foam densification occurred over a large area. Yet, the strength of the top facesheet is maintained, if not increased. Much less densification occurred than in mechanical bending.

the sheet thickness squared for TGM conditions [22]. Eventually, the facesheet becomes too stiff, and  $\Delta\alpha \to 0$  for the entire sandwich. At D=12 mm, significant thickening occurs as well, especially at large bending angles as shown in Fig. 11. However, the bending efficiency is less affected, because the temperature distributions in the top facesheet remains mostly uniform due to the large laser spot size, and the thermal prerequisite for the UM is still met.

Another cause for the different limiting behaviors is the efficiency of the foam densification via the MTGM. As mentioned in Sec. 5.1, densification occurs very locally at D=4 mm, unlike at D=12 mm where a large segment of the foam densifies, as seen in Fig. 11. Therefore, the foam can densify unrestrictedly at D=12 mm, whereas it might locally approach solidification at D=4 mm, reducing the bending efficiency [18].

After reviewing the behavior of sandwich panels at large bending angles, the impact of laser forming on sandwich performance can be examined. The first issue to be examined is facesheet thickening. On one hand, a thickened facesheet increases the strength and stiffness of the sandwich panel. Conversely, the thickened segment has undergone numerous rapid heating and cooling cycles that can cause a material embrittlement [36]. However, since the facesheet thickening occurs over a larger scale and aluminum is less susceptive to detrimental embrittlement effects, it is expected that the top facesheet performance is maintained, if not improved. The second issue is foam densification. At D = 4 mm, the densification resembles the densification observed during laser forming of free-standing metal foam [18]. With an increasing number of scans, the densification becomes more localized and thus minimally affects foam crushability. At  $D = 12 \,\mathrm{mm}$ , the densification is wide-spread, due to the MTGM, as well as the largescale thickening of the top facesheet. Still, the densification is much smaller than in mechanical bending, where the top facesheet deeply penetrates into the foam core and can reduce its thickness by up to 75% [12,13].

5.3 Other Process Conditions. The process window is not limited to the two process conditions that have been compared thus far, but covers the entire spectrum in between. As shown in Fig. 13, any laser spot size between  $D = 4 \,\mathrm{mm}$  and  $D = 12 \,\mathrm{mm}$ yields a successful result (at AE = const.). At each spot size, the bending curve slightly leveled off with an increasing number of laser scans. At  $D = 4 \,\mathrm{mm}$  and  $D = 6 \,\mathrm{mm}$ , the bending curve leveled off more quickly since the TGM, which is more sensitive to facesheet thickening (see Sec. 5.2), was dominant in the top facesheet. Also, the paint wore off faster due to the higher temperatures that developed in the top facesheet. At  $D = 10 \,\mathrm{mm}$  and  $D = 12 \,\mathrm{mm}$ , the bending curves leveled off the least, since the BM, which is less sensitive to facesheet thickening, was dominant in the top facesheet. Also, the temperatures in the top facesheet were the lowest and caused the least amount of paint evaporation. Finally,  $D = 8 \,\mathrm{mm}$  was somewhere in between, and only leveled off at a high number of laser scans.

More insight into the bending efficiency can be obtained by comparing the bending angles achieved by each condition after one and eight laser scans, shown in Fig. 14. After one scan, there was a distinct increase in the bending angle from  $D=4\,\mathrm{mm}$  to  $D = 8 \,\mathrm{mm}$ , which became even more pronounced after 8 scans. Again, the reason is that as the spot size increases, less paint evaporation occurs, and the bending mechanism is less sensitive to facesheet thickening. Additionally, at  $D=4 \,\mathrm{mm}$  and  $D=6 \,\mathrm{mm}$ , facesheet temperatures were very close to melting temperatures (see Fig. 5), hence localized melting could occur, releasing part of the compressive stresses. Figure 14 further shows a slight drop in the bending angle from  $D = 8 \,\mathrm{mm}$  to  $D = 12 \,\mathrm{mm}$  after one laser scan. After eight scans, this trend disappeared, and the bending angles leveled off beyond D = 8 mm. The initial trend is related to the fact that increasing scan speeds at constant input energies reduce heat diffusion time, thereby increasing the temperatures



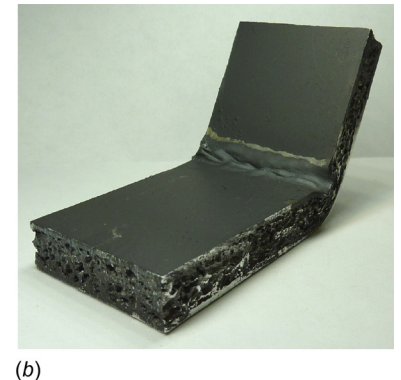


Fig. 12 At D=4 mm, appreciable bending angles can only be obtained by performing parallel scans, as shown in (a), where two scans were performed per scan line and offset by 1 mm. At D=12 mm, large bending angles up to 65 deg and beyond can be obtained over a single scan line, as shown in (b).

and thus the bending angles [37]. This effect is negated after multiple scans, since larger spot sizes experience less paint evaporation and are less sensitive to facesheet thickening.

Laser forming of sandwich panels is not only possible with a range of spot sizes, but there is also a considerable amount of freedom in the choice of the area energy. As shown in Fig. 15, a 40% change in the scan speed (and hence the area energy) still yielded appreciable bending angles. The spot size and the power were maintained at  $D=12\,\mathrm{mm}$  and  $P=800\,\mathrm{W}$ , respectively. Increasing the scan speed caused a drop in the area energy and hence a reduction of the bending angle, a trend that is well captured by the simulation.

**5.4** Numerical Model Comparison. Thus far, all the presented numerical results were generated using an equivalent sandwich model shown in Fig. 2(a). In this section, the equivalent sandwich model is compared with the Kelvin sandwich model shown in Fig. 2(b), in which the cavities of the foam core are explicitly modeled using Kelvin-cell geometries.

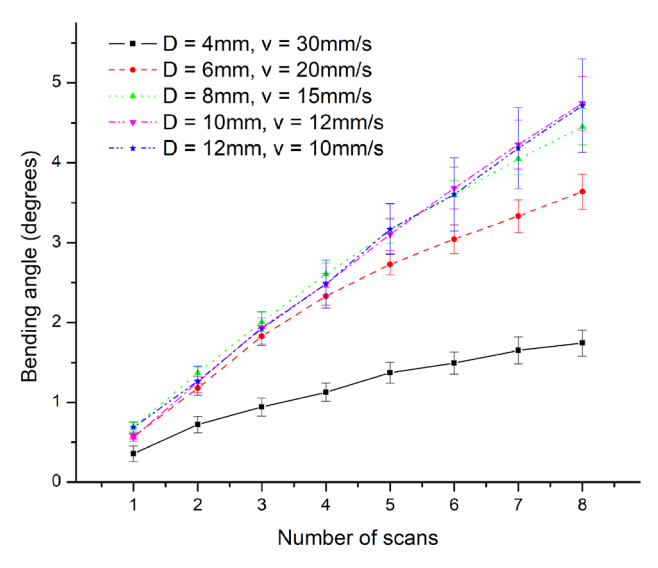


Fig. 13 Experimental bending angles over eight scans at spot sizes ranging from  $D=4\,\mathrm{mm}$  to  $D=12\,\mathrm{mm}$ . The power and area energy are constant at  $P=800\,\mathrm{W}$  and  $AE=6.67\,\mathrm{J/mm^2}$ , respectively. The bending angles are averaged over five specimens, standard errors are shown. At small spot sizes, the bending curves level off more rapidly due to an increased amount of paint evaporation and a higher sensitivity to facesheet thickening.

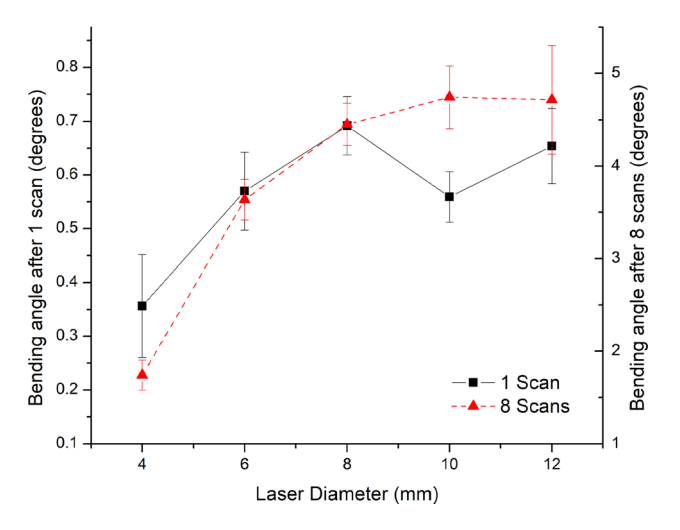


Fig. 14 Experimental bending angles after 1 scan and 8 scans at spot sizes ranging from  $D=4\,\mathrm{mm}$  to  $D=12\,\mathrm{mm}$ . The power and area energy are constant at  $P=800\,\mathrm{W}$  and  $AE=6.67\,\mathrm{J/mm^2}$ , respectively. The bending angles are averaged over five specimens, standard errors are shown.

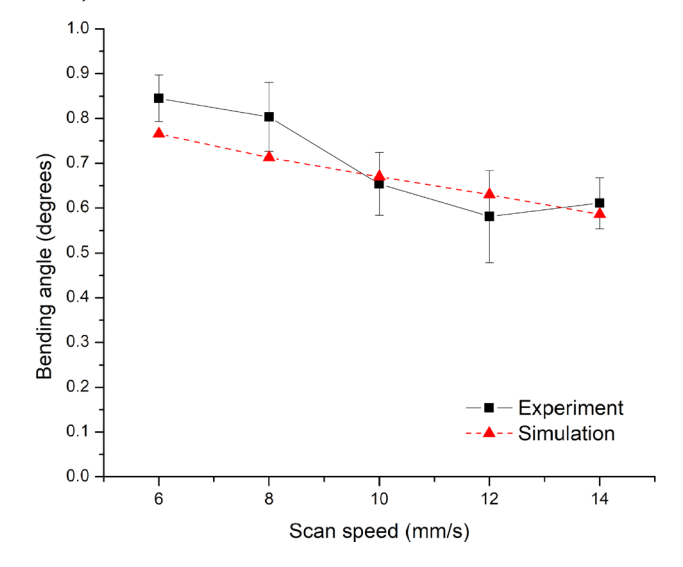


Fig. 15 Experimental and numerical bending angles after a single scan at a spot size of  $D=12\,\mathrm{mm}$  and a power of  $P=800\,\mathrm{W}$ . The experimental results were averaged over five specimens, standard errors are shown. With increasing scan speed, the area energy and, thus, the bending angle decrease. A considerable range of area energies can be used.

**Journal of Manufacturing Science and Engineering** 

NOVEMBER 2018, Vol. 140 / 111015-9

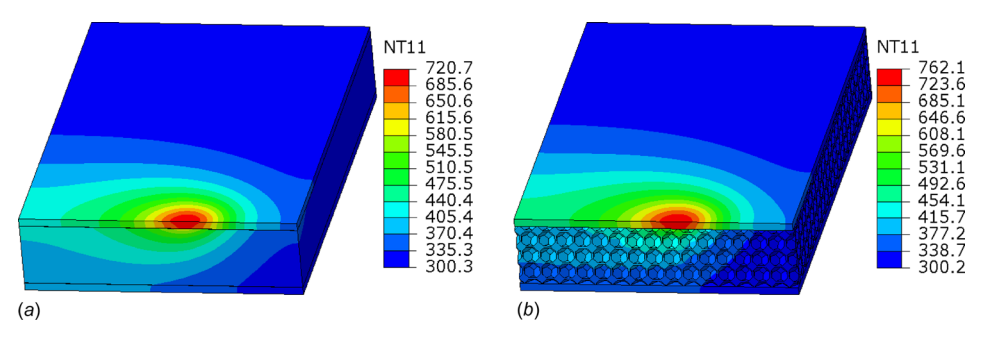


Fig. 16 Temperature distribution in a sandwich specimen scanned at  $D = 12 \,\mathrm{mm}$  and  $v = 10 \,\mathrm{mm/s}$  using a (a) equivalent sandwich model and a (b) Kelvin sandwich model. Half of the specimen is shown due to symmetry.

On one hand, the foam model geometry appears to be less important in sandwich panels than in free-standing foams [17], because the laser absorption in the top facesheet is the same regardless of the foam geometry. Also, the temperature

10 Top facesheet 8 6 Equivalent Model D = 4mm Equivalent Model D = 12mm Kelvin Model D = 4mm -- Kelvin Model D = 12mm 2 Bottom facesheet 0 0 100 200 300 400 500 600 700 Temperature (°C)

Fig. 17 Simulated temperature distributions at a cross section (yz-plane) as the laser passes the section, predicted by the equivalent and Kelvin models, for the conditions  $D=4\,\mathrm{mm}$  with  $v=30\,\mathrm{mm/s}$ , and  $D=12\,\mathrm{mm}$  with  $v=10\,\mathrm{mm/s}$ . In the Kelvin sandwich model, the top facesheet temperatures and the temperature drop across the interface are greater due to the additional geometrical restriction of the heat flow at the interface.

distributions during laser scans are very similar in both models, as shown in Fig. 16 for D = 12 mm, v = 10 mm/s, and P = 800 W.

On the other hand, the foam core geometry does have a significant impact on the heat transfer between the facesheets and the metal foam core. In the equivalent sandwich model there is no geometric restriction to heat flow between the facesheet and metal foam, whereas the heat flow in the Kelvin sandwich model is channeled through thin cell walls. This leads to discrepancies in the temperature gradients as shown in Fig. 17 (analogous to Fig. 5). Due to the geometrical restriction of the heat flow, more heat gets "trapped" in the top facesheet of the Kelvin sandwich model. As a consequence, the top facesheet heats up more and a greater temperature drop establishes across the interface. This discrepancy is more pronounced at  $D=12\,\mathrm{mm}$  than at  $D=4\,\mathrm{mm}$ , since heat has more time to dissipate due to the reduced scan speed [37], thereby rendering the interface property more important.

The foam core geometry also has a significant impact on the mechanical interaction between the facesheets and foam core. In the equivalent sandwich model, the top facesheet thickens the same way everywhere along the laser scan path (see Fig. 8). In the Kelvin sandwich model, on the other hand, the foam core has high geometry-induced stiffness, which locally restricts facesheet expansion, a phenomenon that was also observed in experiments. At sections where a cavity is underneath the facesheet at the scan line (Fig. 18(a)), the facesheet can expand downward unrestrictedly, and significant plastic compressive strain develops in the facesheet. At sections where a cell wall is located underneath the facesheet at the scan line (Fig. 18(b)), the facesheet expansion is restricted and less plastic compressive strains develop. This

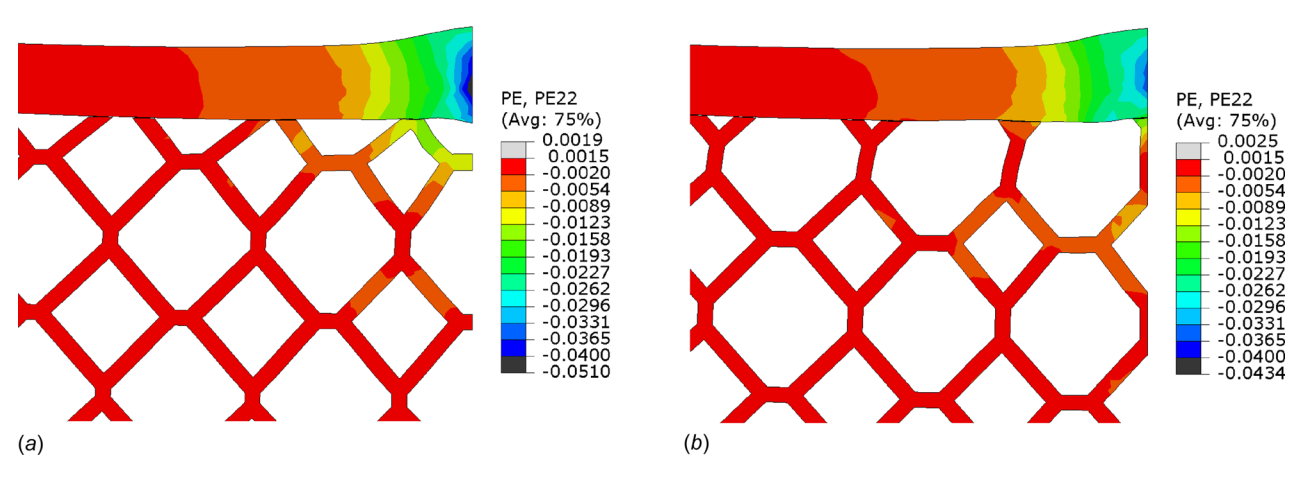


Fig. 18 Plastic strain distribution in the Kelvin sandwich model after a laser scan at D=4 mm with v=30 mm/s. A deformation scaling factor of 10 was used. Half of the specimen is shown due to symmetry. In (a), a cavity is located underneath the face-sheet at the scan line, and the face-sheet can expand downwards unrestrictedly. In (b), a cell wall is located underneath the face-sheet, and the downward expansion of the face-sheet is restricted.

111015-10 / Vol. 140, NOVEMBER 2018

**Transactions of the ASME** 

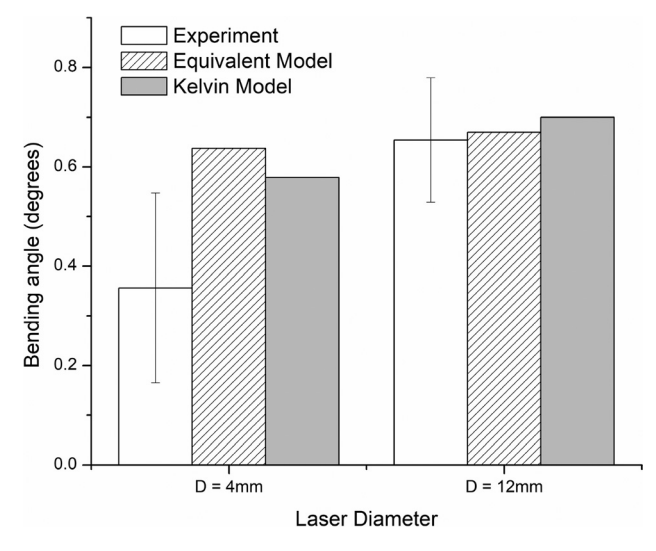


Fig. 19 Experimental and numerical bending angles after a single laser scan at  $D=4\,\mathrm{mm}$  and  $v=30\,\mathrm{mm/s}$ , and  $D=12\,\mathrm{mm}$  and  $v=10\,\mathrm{mm/s}$  ( $P=800\,\mathrm{W}=\mathrm{const.}$ ). The Kelvin model is more sensitive to changes in process conditions due to its higher geometrical accuracy. Both models over-predicted the bending angles at  $D=4\,\mathrm{mm}$  because they did not account for paint evaporation and localized melting.

phenomenon occurs predominantly at  $D=4\,\mathrm{mm}$ , because the facesheet expansion is highly localized at the laser scan line. At  $D=12\,\mathrm{mm}$ , the facesheet thickens over a larger distance from the laser scan line, and the impact of the foam core geometry is reduced.

Due to its increased geometrical accuracy, the Kelvin sandwich model has an increased sensitivity to changes in process conditions, as shown in Fig. 19. Whereas the equivalent sandwich model predicted little difference in bending angle between the small spot size (D=4 mm) and the large spot size (D=12 mm), the Kelvin sandwich model predicted a more significant difference between the two, which more closely agrees with experimental results. Both models over-predicted the bending angles at D=4 mm, since neither of the models account for paint evaporation and possible local melting effects that occur at D=4 mm.

## 6 Conclusions

This study demonstrated that sandwich panels with metal foam core can be laser formed with a wide range of process conditions. It was shown that both the top facesheet and the metal foam core bend via a laser forming mechanism and actively contribute to the bending deformation. The top facesheet bending mechanism depends on the laser spot size and varies between the TGM (for small spot sizes around D=4 mm) and the UM (for large spot sizes around D = 12 mm). The metal foam core bends via the MTGM for all spot sizes. It was also demonstrated that sandwich panels bend more efficiently at large spot sizes than at small spot sizes, since larger segments of the top facesheet and the metal foam contribute to the compressive shortening. Moreover, it was shown that much greater bending angles can be achieved at larger spot sizes, due to the reduced impact of facesheet thickening on bending mechanism efficiency. Finally, it was shown that Kelvin sandwich models yield better predictions of bending angles and the facesheet/foam core interaction than equivalent sandwich models, due to their higher geometrical accuracy.

From this study, it became clear that the facesheet/foam core interface plays a central role in laser forming of sandwich panels. Different adhesion types might significantly affect the heat transfer and the mechanics, and hence change the outcome of the laser forming process.

## Acknowledgment

The supply of aluminum foam sandwich material from Havel metal foam GmbH is greatly appreciated.

## **Funding Data**

- The Extreme Science and Engineering Discovery Environment (XSEDE) Stampede through allocation TG-DDM160002, which is supported by the National Science Foundation (ACI-1548562 [38]).
- The National Science Foundation under a GOALI (Grant No. CMMI- 1725980).

#### **Nomenclature**

A = absorption coefficient

AE = area energy

c = geometry correction factor

D = laser beam diameter

E =Young's Modulus

F =yield surface parameter

G = interface conductance

 $G_c$  = corrected interface conductance

 $h_{\sigma}$  = tangent modulus in uniaxial compression

 $h_p$  = tangent modulus in hydrostatic compression

 $\hat{H}$  = hardening modulus

I =moment of area

l = half beam length

M =bending moment

P = laser power

R = radius of curvature

S = bending stiffness

T = temperature

Y = yield strength

 $\dot{Y}$  = rate of change of yield strength

 $s_0$  = sheet thickness

v =laser scan speed

x = x-coordinate

y = y-coordinate

z = z-coordinate

 $\alpha$  = aspect ratio of yield surface

 $\delta = \text{vertical deflection}$ 

 $\varepsilon = strain$ 

 $\varepsilon_{ii} = \text{uniaxial strain components}$ 

 $\dot{\varepsilon}_{ij}^p = \text{plastic strain rate}$ 

 $\rho = \text{density}$ 

 $\dot{\rho}_0 = \text{initial density}$ 

 $\sigma = \text{stress}$ 

 $\sigma_e$  = Von Mises' equivalent stress

 $\sigma_m$  = mean stress

 $\hat{\sigma} = \text{equivalent stress}$ 

## References

- Gibson, L. J., and Ashby, M. F., 1988, Cellular Solids: Structure & Properties, Pergamon. Oxford, UK.
- [2] Ashby, M. F., Evans, A. G., Fleck, N. A., Gibson, L. J., Hutchinson, J. W., and Wadley, H. N. G., 2000, *Metal Foams: A Design Guide*, Butterworth-Heineman, Washington DC.
- [3] Srivastava, V. C., and Sahoo, K. L., 2007, "Processing, Stabilization and Applications of Metallic Foams. Art of Science," Mater Sci-Poland, 25(3), pp. 733–753.
- [4] Claar, T. D., Yu, C. J., Hall, I., Banhart, J., Baumeister, J., and Seeliger, W., 2000, "Ultra-Lightweight Aluminum Foam Materials for Automotive Applications," SAE Paper No. 2000-01-0335.
- [5] Han, M. S., Min, B. S., and Cho, J. U., 2014, "Fracture Properties of Aluminum Foam Crash Box," Int. J. Automot. Technol., 15(6), pp. 945–951.
- [6] Banhart, J., and Seeliger, H. W., 2012, "Recent Trends in Aluminum Foam Sandwich Technology," Adv. Eng. Mater., 14(12), pp. 1082–1087.
  [7] Kremer, K., 2004, "Metal Foams for Improved Crash Energy Absorption in
- [7] Kremer, K., 2004, "Metal Foams for Improved Crash Energy Absorption in Passenger Equipment," *National Academies of Sciences, Engineering, and Medicine*, Washington DC.

**Journal of Manufacturing Science and Engineering** 

NOVEMBER 2018, Vol. 140 / 111015-11

- [8] Crupi, V., Epasto, G., and Guglielmino, E., 2013, "Comparison of Aluminium Sandwiches for Lightweight Ship Structures: Honeycomb Vs. foam," Mar. Struct., 30, pp. 74–96.
- [9] Hebsur, M., Noebe, R., and Revilock, D., 2003, "Impact Resistance of Light-weight Hybrid Structures for Gas Turbine Engine Fan Containment Applications," J. Mater. Eng. Perform., 12(4), pp. 470–479.
- [10] Hanssen, A. G., Girard, Y., Olovsson, L., Berstad, L., and Langseth, M., 2006, "A Numerical Model for Bird Strike of Aluminium Foam-Based Sandwich Panels," Int. J. Impact Eng., 32(7), pp. 1127–1144.
- [11] Banhart, J., and Seeliger, H. W., 2008, "Aluminium Foam Sandwich Panels: Manufacture, Metallurgy and Applications," Adv. Eng. Mater., 10(9), p. 793.
- [12] Zu, G. Y., Lu, R. H., Li, X. B., Zhong, Z. Y., Ma, X. J., Han, M. B., and Yao, G. C., 2013, "Three-Point Bending Behavior of Aluminum Foam Sandwich With Steel Panel," Trans. Nonferrous Met. Soc. China, 23(9), pp. 2491–2495.
- [13] D'Urso, G., and Maccarini, G., 2011, "The Formability of Aluminum Foam Sandwich Panels," Int. J. Mater. Form, 5(3), pp. 243–57.
- [14] Contorno, D., Filice, L., Fratini, L., and Micari, F., 2006, "Forming of Aluminum Foam Sandwich Panels: Numerical Simulations and Experimental Tests," J. Mater. Process. Technol., 177(1–3), pp. 364–367.
- [15] Li, Z., Zheng, Z., Yu, J., Qian, C., and Lu, F., 2014, "Deformation and Failure Mechanisms of Sandwich Beams Under Three-Point Bending at Elevated Temperatures," Compos. Struct., 111, pp. 285–290.
- [16] Mata, H., Santos, A., Parente, M., Valente, R., Fernandes, A., and Jorge, N., 2013, "Study on the Forming of Sandwich Shells With Closed-Cell Foam Cores," Int. J. Mater. Form, 7(4), pp. 413–424.
- [17] Bucher, T., Bolger, C., Zhang, M., Chen, C., and Yao, Y. L., 2016, "Effect of Geometrical Modeling on Prediction of Laser-Induced Heat Transfer in Metal Foam," ASME J. Manuf. Sci. Eng., 138(12), p. 121008.
- [18] Bucher, T., Young, A., Zhang, M., Chen, C. J., and Yao, Y. L., 2018, "Thermally Induced Mechanical Response of Metal Foam During Laser Forming," ASME J. Manuf. Sci. Eng., 140(4), p. 041004.
  [19] Santo, L., Guglielmotti, A., and Quadrini, F., 2010, "Formability of Open-Cell
- [19] Santo, L., Guglielmotti, A., and Quadrini, F., 2010, "Formability of Open-Cell Aluminium Foams by Laser," ASME Paper No. MSEC2010-34282.
- [20] Guglielmotti, A., Quadrini, F., Squeo, E. A., and Tagliaferri, V., 2009, "Laser Bending of Aluminum Foam Sandwich Panels," Adv. Eng. Mater, 11(11), pp. 902–906.
- [21] Hibbeler, R. C., and Vijay, K. S., 2013, Mechanics of Materials, Pearson Education, London.
- [22] Vollertsen, F., 1993, "The Mechanisms of Laser Forming," CIRP Ann., 42(1), pp. 301–304.
- [23] Chen, W., Hao, H., Chen, S., and Hernandez, F., 2015, "Performance of Composite Structural Insulated Panel With Metal Skin Subjected to Blast Loading," Mater. Des., 84, pp. 194–203.

- [24] Camanho, P. P., Davila, C. G., and De Moura, M. F., 2003, "Numerical Simulation of Mixed-Mode Progressive Delamination in Composite Materials," J. Compos. Mater., 37(16), pp. 1415–438.
- [25] Wang, H., Yao, Y. L., and Chen, H., 2015, "Removal Mechanism and Defect Characterization for Glass-Side Laser Scribing of CdTe/CdS Multilayer in Solar Cells," ASME J. Manuf. Sci. Eng., 137(6), p. 061006.
- [26] Turon, A., Davila, C. G., Camanho, P. P., and Costa, J., 2007, "An Engineering Solution for Mesh Size Effects in the Simulation of Delamination Using Cohesive Zone Models," Eng. Fract. Mech., 74(10), pp. 1665–1682.
- [27] Skidmore, M., and Johnson, R., 1989, "Thermal Contact Conductance of Various Metals at Elevated Temperatures," 24th Thermophysics Conference, Buffalo, NY, June 12–14, pp. 1–8.
- [28] Liu, D. H., and Shang, X. C., 2013, "The Physical-Mechanism Based High-Temperature Thermal Contact Conductance Model With Experimental Verification," Chin. Phys. Lett., 30(3), p. 036501.
- [29] Dou, R., Ge, T., Liu, X., and Wen, Z., 2016, "Effects of Contact Pressure, Interface Temperature, and Surface Roughness on Thermal Contact Conductance Between Stainless Steel Surfaces Under Atmosphere Condition," Int. J. Heat Mass Transfer, 94, pp. 156–163.
- [30] Spittel, T., Spittel, M., and Warlimont, H., 2011, Non-Ferrous Alloys—Light Metals Vol.VIII/2C2, Springer, Berlin, Germany.
- [31] Deshpande, V., and Fleck, N., 2000, "Isotropic Constitutive Models for Metallic Foams," J. Mech. Phys. Solids, 48.6(6–7), pp. 1253–1283.
- [32] Li, W., and Yao, Y. L., 2000, "Numerical and Experimental Study of Strain Rate Effects in Laser Forming," ASME J. Manuf. Sci. Eng., 122(3), p. 445.
- [33] Steen, W. M., 1998, Laser Material Processing, Springer, London.
- [34] Edwardson, S. P., French, P., Dearden, G., Watkins, K. G., and Cantwell, W. J., 2005, "Laser Forming Fibre Met. Laminates," Lasers Eng., 15(3), pp. 233–255.
- [35] Bartkowiak, K., Dearden, G., Edwardson, S. P., and Watkins, K. G., 2004, "Development of 2D and 3D Laser Forming Strategies for Thin Section Materials Using Scanning Optics," 23rd International Congress on Applications of Lasers & Electro-Optics (ICALEO 2004), San Francisco, CA, Oct. 4–7, Paper No. 559.
- [36] Cheng, J., and Yao, Y. L., 2002, "Microstructure Integrated Modeling of Multiscan Laser Forming," ASME J. Manuf. Sci. Eng., 124(2), pp. 379–388.
- [37] Li, W., and Yao, Y. L., 2001, "Laser Forming With Constant Line Energy," Int. J. Adv. Manuf. Technol., 17(3), pp. 196–203.
- [38] Towns, J., Cockerill, T., Dahan, M., Foster, I., Gaither, K., Grimshaw, A., Hazlewood, V., Lathrop, S., Lifka, D., Peterson, G. D., Roskies, R., Scott, J. R., and Wilkins-Diehr, N., 2014, "XSEDE: Accelerating Scientific Discovery," Comput. Sci. Eng., 16(5), pp. 62–74.